Journal of Catalysis 262 (2009) 65–72

Contents lists available at ScienceDirect

Journal of Catalysis

www.elsevier.com/locate/jcat

Transient behavior of Cu/ZnO-based methanol synthesis catalysts

Peter C.K. Vesborg [a,b], Ib Chorkendorff [a], Ida Knudsen [a], Olivier Balmes [b], Jesper Nerlov [b], Alfons M. Molenbroek [b], Bjerne S. Clausen [b], Stig Helveg [b,*]

[a] CINF, Dept. of Physics, NanoDTU, Technical University of Denmark, DK-2800 Kgs. Lyngby, Denmark
[b] Haldor Topsøe A/S, Nymøllevej 55, DK-2800 Kgs. Lyngby, Denmark

ARTICLE INFO

Article history:
Received 23 July 2008
Revised 18 November 2008
Accepted 30 November 2008
Available online 18 January 2009

Keywords:
Cu/ZnO catalyst
Methanol synthesis
Transient
Nanoparticles
ETEM

ABSTRACT

Time-resolved measurements of the methanol synthesis reaction over a Cu/ZnO-based catalyst reveal a transient methanol production that depends on the pretreatment gas. Specifically, the methanol production initially peaks after a pretreatment with an intermediate mixture of H_2 and CO (20–80% H_2 in CO). The activity measurements are compared to Environmental Transmission Electron Microscopy (ETEM) observations of Cu nanoparticles supported on ZnO during exposure to comparable reaction conditions. The ETEM images reveal a gas-dependent morphology of the Cu nanoparticles with a marked flattening for a gas mixture of H_2:CO = 1:1. The gas-dependent morphology of the Cu nanoparticles provides a consistent explanation of the observed coupling between the transient methanol production and pretreatment conditions within the framework of the dynamic microkinetic model by Ovesen et al. [J. Catal. 168 (1997) 133–142].

1. Introduction

Methanol is becoming an increasingly important chemical and is considered as an energy carrier in future energy infrastructure [1]. Industrial methanol synthesis is accomplished by catalytically converting *syngas* (a mixture of H_2, CO and CO_2) over a $Cu/ZnO/Al_2O_3$ catalyst via the following reactions:

$$CO_2 + 3H_2 \rightleftharpoons CH_3OH + H_2O, \quad (1)$$

$$CO + H_2O \rightleftharpoons CO_2 + H_2. \quad (2)$$

Hydrogenation of CO_2 is demonstrated to be the important route to methanol using Cu/ZnO-based catalysts by means of isotope labelling experiments [2,3]. Moreover, experiments with Cu single and poly-crystals with and without CO_2 in the CO/H_2 feed indicate that direct CO hydrogenation is not significant [4]. In hydrogenation of CO_2, steam is an unavoidable byproduct and the CO component in syngas mainly serves to suppress steam via the water–gas shift reaction (2) [5–8].

Industrial Cu/ZnO-based catalysts have high activity and selectivity towards methanol so the synthesis is performed under mild conditions with pressures of about 70 bar and temperatures of about 500 K [9]. Copper alone may work as a methanol synthesis catalyst, but the activity increases significantly for Cu supported by ZnO, which by itself has only negligible methanol synthesis activity. The nature of the metal–support synergy in the Cu/ZnO system is much debated [10] and several possible explanations for the Cu/ZnO synergy are proposed including support-induced strain in Cu [11,12], Zn-species segregation onto Cu [13], Cu–Zn alloy formation [10,14,15] and gas-dependent morphology of Cu on ZnO [16,17]. The relative importance of the different effects is still a subject of debate and it is possible that several effects are relevant simultaneously depending on catalyst preparation and reaction environment [10].

Important for the discussion of Cu-based methanol synthesis catalysts is the introduction of *in situ* characterization techniques. Specifically, *in situ* Extended X-ray Absorption Fine Structure (EXAFS) measurements show that the Cu nanoparticles are present in the metallic state during methanol synthesis [18] and that the shape of the Cu particles is dependent on the composition of the methanol synthesis gas environment (Fig. 1) [16,17]. The dynamic morphology of the Cu particles is attributed to gas-induced changes in the Cu/ZnO interface energy [16,17]. Ovesen et al. established a microkinetic model that incorporates the gas-induced shape change in the Cu nanoparticles [19]. The model describes the activity of the Cu nanoparticles as a function of the type and concentration of exposed low-index Cu facets and includes the relative methanol activity of the different facets from surface science data. Specifically, the model suggests a shape-activity relationship in which the flatter Cu nanoparticles have a higher methanol synthesis activity than more spherical particles due to their higher surface area and higher fraction of high-index surface facets. By including the gas-dependent Cu nanoparticle shape, the microkinetic model can describe the measured methanol rates under differ-

* Corresponding author.
E-mail address: sth@topsoe.dk (S. Helveg).

0021-9517/$ – see front matter
doi:10.1016/j.jcat.2008.11.028

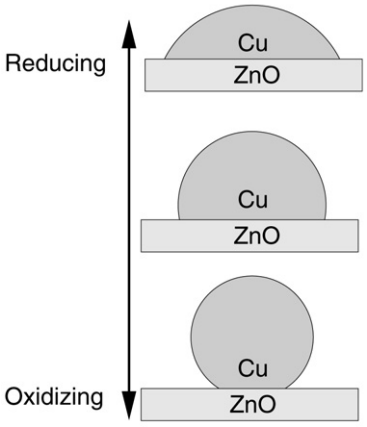

Fig. 1. Illustration of the dynamic morphology of Cu particles on a ZnO support with changes in the reduction potential of the gas environment [17]. During methanol synthesis the gas environment is more reducing or oxidizing depending on the steam concentration.

ent methanol synthesis conditions quite well [19]. Moreover, the shape-activity relationship also provides a consistent explanation for the observation of transients in the methanol production over Cu/ZnO-based catalysts [20].

In the present article, we address the relationship between the transient methanol production and the pretreatment gas composition. Time-resolved measurements of the methanol production show that a maximum over-production occurs after pretreatment in an intermediate mixture of H_2 and CO (20–80% H_2 in CO). The activity measurements are compared to Environmental Transmission Electron Microscopy (ETEM) observations of Cu on nanoparticles supported on ZnO during exposure to reaction conditions mimicking the pretreatment and methanol synthesis conditions. Previous studies have shown that ETEM is indeed capable of resolving gas-dependent nanoparticle shapes *in situ* [21–23]. The comparison reveals that the relationship between the transient methanol production and pretreatment conditions can be explained by a gas-dependent Cu nanoparticle morphology by assuming a shape-activity relationship as in [19]. Surprisingly the findings reveal that the most flat and active Cu nanoparticles are formed during exposure to an intermediate gas mixture of H_2 and CO and not of the pure gas components.

2. Experimental

2.1. Methanol synthesis measurements

Measurements of the methanol production from syngas over a $Cu/ZnO/Al_2O_3$ catalyst were carried out in a laminar flow tube reactor. The gas handling system was made from 1/4″ stainless steel tubing with welded connections and VCR fittings. During experiments the whole setup was kept at 348 K to minimize sticking of H_2O and methanol. All flow controllers were calibrated for their respective gasses as well as for operation at 348 K. The reactor consisted of a 10 cm long and 1/4″ wide Cu tube in which the catalyst was loaded between plugs of pyrex glass wool. Three thermocouples were fitted to the reactor tube and the temperature control in the reactor was estimated to be better than ±2 K. Time-resolved gas detection was done using a quadrupole mass spectrometer (QMS) with a secondary electron multiplier detector fitted to the system using a glass capillary sniffer [24]. The whole system was He leak-tested and blank runs using only pyrex wool as a sample were performed to ensure that the system alone had no detectable methanol synthesis activity.

Each experiment was carried out using a sample consisting of 1 g of crushed $Cu/ZnO/Al_2O_3$ catalyst [25]. The sample was initially activated by heating at 1 K/min to 500 K in a 40:30:5:25 H_2:CO:CO_2:He mixture at 4 bar. After this activation procedure, the sample was exposed to a pretreatment gas consisting of a mixture of H_2 and CO at a total pressure of 4 bar and a flow of 100 Nml/min for 2 h at 500 K. Different ratios of H_2 and CO in the pretreatment gas were used in different experiments. Finally the sample was exposed to syngas at 500 K, 4 bar and 100 Nml/min. The composition of the syngas was the same as for the activation gas. At the chosen flow rate, the setup had a delay of about 70 s from the change-over from the pretreatment gas to the syngas before a methanol was observed by monitoring $m/Z = 31$ the QMS. The transient methanol peak always occurred at about 120 s after the change-over.

2.2. Environmental Transmission Electron Microscopy (ETEM)

The ETEM experiments were carried out using a Philips CM300 ST FEG-TEM instrument equipped with a differentially pumped environmental cell [26]. The instrument allows solid catalysts to be imaged *in situ* with a resolution limit of ca. 0.14 nm during exposure to reactive gasses at pressures up to ca. 10 mbar and temperatures up to approximately 1200 K. ETEM images were recorded using a highly sensitive, fast-scan CCD camera (Tietz F114). Furthermore, the microscope is equipped with a Gatan Imaging Filter (GIF-2000) allowing Electron Energy Loss Spectroscopy (EELS) to be carried out.

In Transmission Electron Microscopy (TEM) of Cu/ZnO-based methanol synthesis catalysts, the unambiguous distinction between Cu and ZnO nanoparticles is often hampered by their comparable sizes and mass-thickness contrast. To mitigate this problem, a model Cu/ZnO catalyst with 20–80 nm wide and well-facetted ZnO particles was used. Recently, thorough TEM experiments showed that model Cu/ZnO catalysts indeed provide structural information representative for the industrial-type catalysts [27] and in this work no activity measurements were therefore performed on the model catalyst. The model catalyst was prepared by heating a mix of copper acetyl acetonate with ZnO (Advanced Nanotechnology Limited, Australia) to 473 K followed by calcination in air to 673 K. The resulting model catalyst precursor consisted of CuO/ZnO with a few percent Cu loading as estimated by EELS.

Samples for the ETEM experiments were prepared by dispersing the crushed, calcined powder onto plasma-cleaned TEM grids of stainless steel and a grid was loaded into the microscope using a Gatan single-tilt heating holder (Model 628) in each experiment. After insertion into the microscope, each sample was initially subjected to a reduction procedure in which the sample was heated to 553 K in 2 mbar H_2 for 30–60 min. The temperature was measured by a thermocouple mounted on the furnace of the heating holder. EEL spectroscopy showed (in accordance with previous results [28]) that this procedure effectively transforms the CuO in the calcined catalyst to metallic Cu. Fig. 2 shows that the resulting Cu particles had diameters in the range 4–8 nm and were easily distinguished from the larger ZnO particles. Following the initial reduction in H_2, the sample was exposed to the gas mixture of interest at 500 K. Specifically, the Cu/ZnO samples were exposed to H_2, CO or mixtures thereof to mimic the reducing pretreatment conditions or to gas mixtures containing CO_2 (including syngas) and H_2O to mimic the methanol synthesis conditions. Table 1 describes the different gas mixtures in detail. For all experiments with CO-containing gasses, the gas was led through a carbon filter located in front of the inlet to the environmental cell to prevent Ni-contamination from $Ni(CO)_4$ residues in the gas, which would otherwise have contaminated the sample in the microscope. H_2O was dosed from a separate liquid reservoir purified by freeze–pump–thaw cycles. After each change-over from the reducing H_2

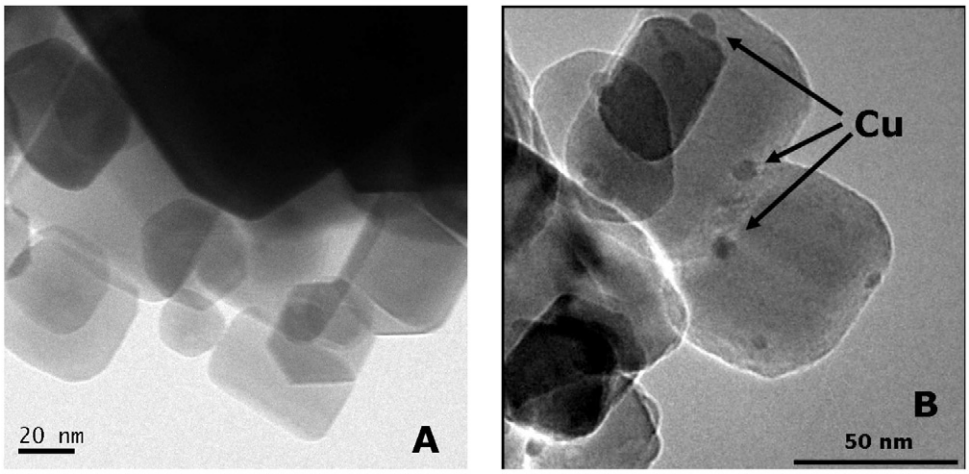

Fig. 2. (A) A TEM image of the pure ZnO support material showing the typical size and crystal shape of the bare ZnO particles. (B) An ETEM image of the Cu/ZnO model catalyst in 2 mbar H_2, 500 K showing the Cu nanoparticles as darker spots with diameters of 4–8 nm situated on the ZnO particles.

Table 1
The composition of the gas mixtures used in the ETEM experiments.

Gas	Partial pressure (mbar)			
	H_2	CO	H_2O	CO_2
50:50 CO:H_2	1	1	0	0
5:95 CO:H_2	1.9	0.1	0	0
CO	0	2	0	0
H_2	2	0	0	0
Dry syngas	1.8	0.1	0	0.1
5:95 CO_2:H_2	1.9	0	0	0.1
50:50 CO_2:H_2	1	0	0	1
Wet syngas	1.8	0.1	1	0.1
Wet 5:95 CO:H_2	1.9	0.1	1	0
Wet H_2	2	0	1	0

gas to the gas mixture of interest, the sample was left for at least 30 min in the gas environment at 500 K before ETEM imaging was performed. Monitoring the particle shapes over several subsequent hours revealed no measurable shape changes as a function of time indicating fast shape equilibration within the 30 min. The sample was searched close to the grid center for Cu particles which could be observed in *profile view* with minimal overlap between the Cu particle and the ZnO support. During image acquisition, the beam intensity was kept below 0.3 A/cm^2, which was sufficiently low to avoid affecting the particle shape over an extended exposure to the electron beam.

3. Results

3.1. Methanol synthesis activity measurements

A series of experiments was carried out to investigate how the composition of the reducing pretreatment gas affects the transient methanol activity. Fig. 3 shows the measured methanol signal as a function of time after the transition from the pretreatment gas to syngas. Methanol production is observed after about 70 s and it approaches a constant asymptotic level after a transient period of about 15 min. For pretreatment with a gas consisting of H_2 and CO with 4–90% CO, the methanol signal increases fast to a transient maximum level after 135 s followed by a decay to a lower constant asymptotic value at later times. The magnitude of the transient methanol production depends strongly on the pretreatment gas composition. Fig. 4 shows the transient methanol production versus the pretreatment gas composition. The transient methanol production is measured as the peak height defined as the difference between the transient methanol activity at time = 135 s and the constant asymptotic level reached after 15 min (Fig. 3). Specifically, Fig. 4 shows that there is a significant transient over-production of

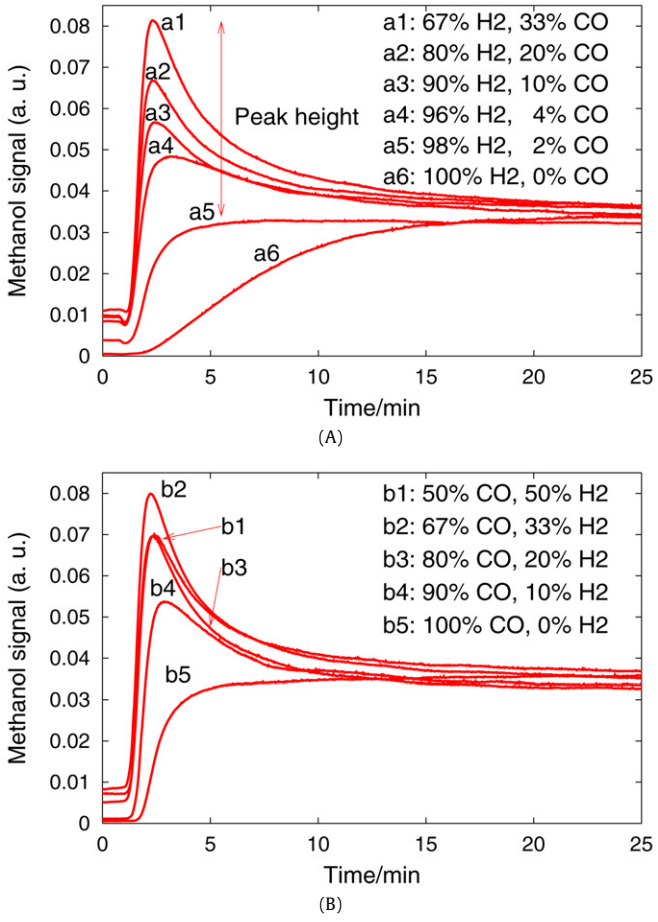

Fig. 3. Methanol production over the Cu/ZnO/Al_2O_3 catalyst as a function of time after different pretreatments. In the pretreatments, the ratio of CO and H_2 is varied with low CO concentrations in (A) and low H_2 concentrations in (B). After a pretreatment, the gas mixture is changed to syngas at time = 0 and the methanol production is monitored over time by the QMS. In (A), the transient methanol production (the peak height) is defined as the difference between the methanol signal at time = 135 s and the constant asymptotic level reached after 15 min. In all experiments, the pressure is 4 bar and the temperature was 500 K.

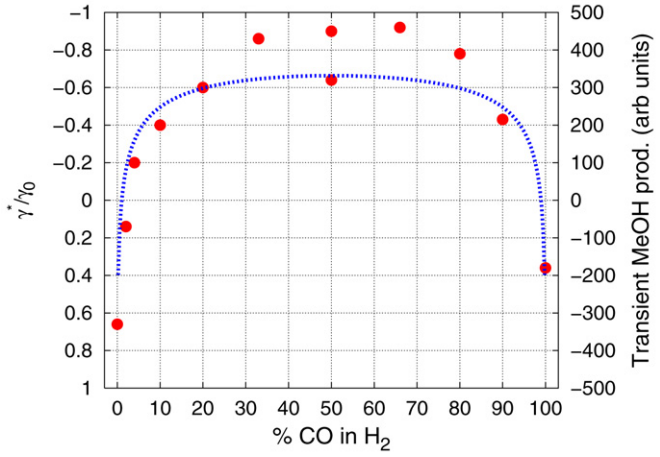

Fig. 4. Comparison of the measured transient methanol production for the Cu/ZnO/Al_2O_3 catalyst and the Cu nanoparticle shape (γ^*/γ_0) versus the composition of the pretreatment gas environment. The transient methanol production for each activity experiment is shown by a dot and the curve represents a least-square fit of the transient methanol production using Eq. (8) with ($P_{H_2O}P_{CO_2}$) as fitting parameter (best fit is for ($P_{H_2O}P_{CO_2}$) = 0.004 mbar^2).

methanol for pretreatment environments containing *both* CO and H_2 in mixtures containing about 20–80% CO and that a maximum in the methanol over-production is obtained for a pretreatment gas of H_2:CO ~ 1:1. For gas compositions outside the range 4–90% CO in H_2, i.e. pure H_2, pure CO and 2% CO in H_2, a transient maximum is not observed and instead the methanol production approaches the asymptotic level monotonously. It is noted that the asymptotic methanol production is approached faster following pretreatments with gasses containing CO than after a pretreatment with pure H_2.

3.2. ETEM experiments

The ETEM experiments allow, the morphology of the Cu nanoparticles in the model catalyst to be studied *in situ* during exposure to gas environments mimicking the pretreatment as well as methanol synthesis conditions. Fig. 5 shows representative ETEM images of Cu nanoparticles on ZnO during exposure to different gas mixtures at a total pressure of 2 mbar and 500 K. Qualitatively, the Cu nanoparticles appear to be more flat under more reducing conditions and more spherical during exposure to more oxidizing gasses. To substantiate these observations, a larger set of images is analyzed for each sample (Table 2). Because the particles were found to rapidly change shape with changes in gas composition and because no further changes were observed during continued ETEM imaging, the particle shapes are assumed to be equilibrated and the Wulff construction framework [29,30] is used to characterize the particle shapes.

In the Wulff construction framework, the three-dimensional shape of the supported nanoparticles is given by the Cu surface and Cu/ZnO interface free energies. In the following, we focus on the effective interface energy, γ^*, for Cu nanoparticles adsorbed on ZnO, because this parameter was previously suggested as an essential parameter for the shape-activity relationship for Cu/ZnO-based catalysts in methanol synthesis [19]. γ^* is the difference between the interface energy (γ_{int}) and the surface energy of the support (γ_{sup}): $\gamma^* = \gamma_{int} - \gamma_{sup}$. The work of adhesion W_{adh} is the work needed to detach Cu from ZnO and is given by: $W_{adh} = \gamma_{sup} + \gamma_0 - \gamma_{int}$, where γ_0 is the free surface energy of Cu. These expressions relate γ^* and W_{adh} by:

$$\frac{W_{adh}}{\gamma_0} = 1 - \frac{\gamma^*}{\gamma_0}. \tag{3}$$

The ratio γ^*/γ_0 can be measured directly from the two-dimensional projected profile-view ETEM images of the Cu nanoparticles (Fig. 6): Firstly, the *Wulff circle* is determined as the circle which best fits the observed corners of the particle. Since the corners represent sites of approximately similar surface energy, the center of the Wulff circle approximates the Wulff point. Secondly, the distance from the Wulff point to the top facet of the particle (a) and the distance to the particle-substrate interface (b) is measured in a direction orthogonal to the Cu/ZnO interface. According to the Wulff construction [29,30], the ratio b/a is given by:

$$b/a \simeq \frac{\gamma^*}{\gamma_0}. \tag{4}$$

Thus, b/a is a measurable estimator for γ^*/γ_0 and hence the work of adhesion normalized to γ_0 (Eq. (3)). We use the term "flat" to refer to particles with a small height and broad metal–support interface corresponding to a low or even negative b/a ratio. A "flat" particle in this context does, therefore, not need to have any flat facets at all.

The Wulff circle analysis is done for N different particles in each gas mixture. In the present samples, the Cu nanoparticles are ~4–8 nm in diameter. The ETEM results show no significant dependence on size, so the results for b/a and W_{adh} (calculated via Eq. (3)) in Table 2 and Fig. 6 are averaged for all particles observed in each gas environment. Specifically, the results for b/a and W_{adh} are presented as weighted averages with the individual weight factors taken as the squared inverse of the estimated uncertainty for b/a in each measurement. In Table 2, the first four rows contain the results for the ETEM experiments using highly reducing gasses mixed of H_2 and CO and the lower six rows show the ETEM results for experiments using gasses that also contained CO_2 and/or H_2O. In order to describe the different gas environments, we introduce Γ_1, Γ_2 and their product Γ to quantify the reduction potential of the different gas mixtures:

$$\Gamma_1 = \frac{P_{H_2}}{P_{H_2O}},$$
$$\Gamma_2 = \frac{P_{CO}}{P_{CO_2}},$$
$$\Gamma = \Gamma_1\Gamma_2, \tag{5}$$

i.e., a high $\Gamma_{(i)}$ value corresponds to a more reducing mixture and a low $\Gamma_{(i)}$ corresponds to a more oxidizing mixture. Furthermore, the different gas environments are characterized by Γ_{frozen}, calculated by using Eq. (5) for the gas mixture entering the ETEM assuming that the water–gas shift reaction is negligible, and by $\Gamma_{equilibrium}$, calculated as the Γ value for the gas mixture entering the ETEM with the water–gas shift reaction at equilibrium at the catalyst surface. In Table 2, the gas environments are ranked according to their $\Gamma_{equilibrium}$ values. The value of Γ at the catalyst surface in the ETEM experiment is not directly measurable but must be between Γ_{frozen} and $\Gamma_{equilibrium}$. Finally, we note that even in the least reducing of the gas mixtures, the ETEM images show no visible indications of re-oxidation of Cu in the form of a mass–thickness contrast change such as a brighter brim around the nanoparticles. Bulk re-oxidation would also be surprising because for the reaction

$$H_2(g) + CuO(s, bulk) \leftrightharpoons Cu(s, bulk) + H_2O(g),$$

the ΔG value is −103 kJ/mol at 500 K and $P_{H_2} = P_{H_2O}$.

The results from the quantitative analysis (Table 2 and Fig. 6) of the larger set of observed Cu nanoparticles clearly show that the nanoparticle shape depends on the gas composition. The average b/a values support the general trend that the least reducing gasses are associated with more spherical particles (high b/a values), whereas the more reducing gasses result in more flat,

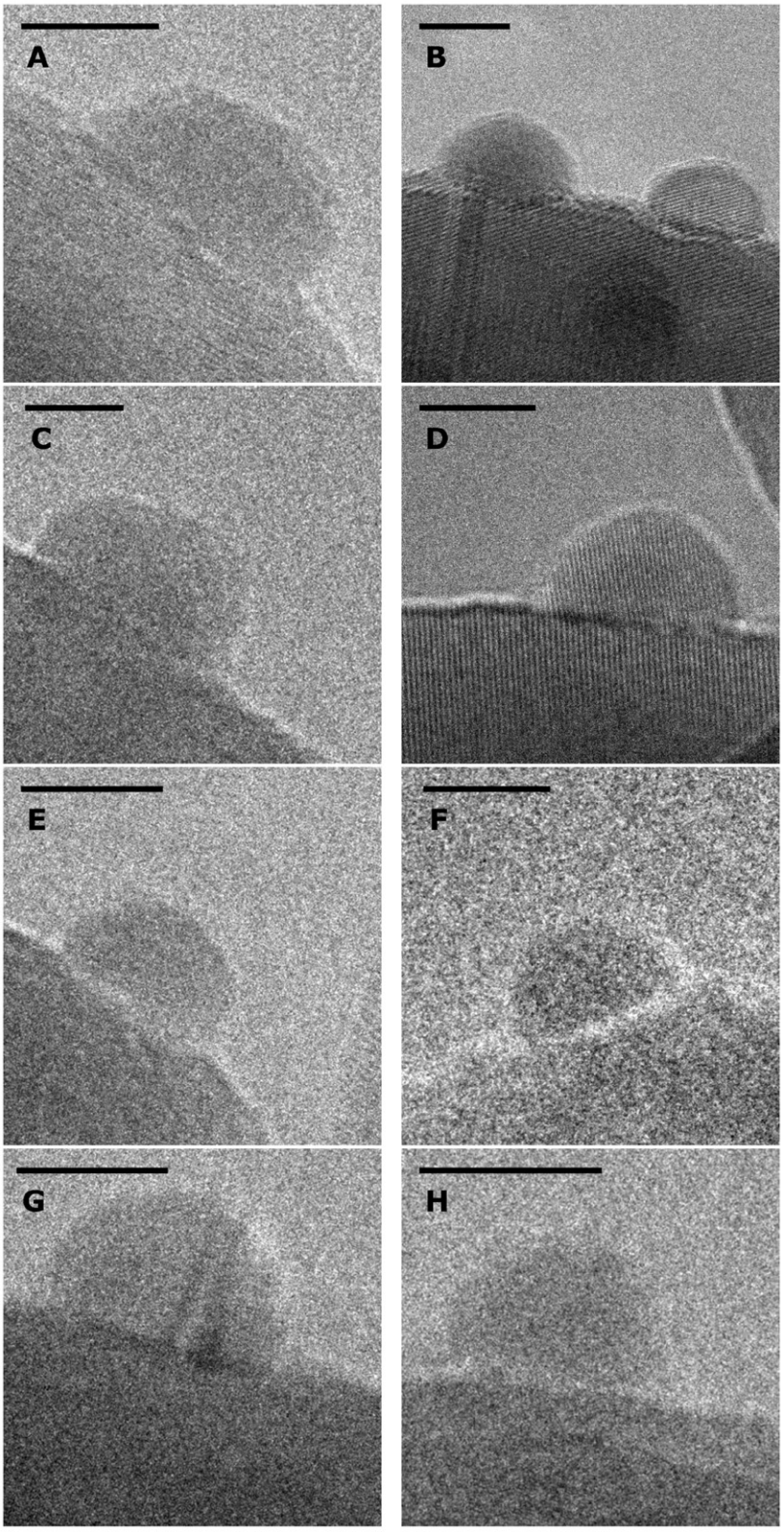

Fig. 5. Representative ETEM images of Cu nanoparticles on ZnO obtained *in situ* during exposure to 2 mbar gas at 500 K. The gas compositions are: (A) 50:50 CO:H_2, (B) CO, (C) H_2, (D) 5:95 CO:H_2, (E) dry syngas, (F) 50:50 CO_2:H_2, (G) wet syngas, (H) wet H_2. Scale bars are 5 nm.

semi-spherical particles (low b/a values). Furthermore the variations in the average b/a values demonstrate that particularly the interface energy is gas-dependent. The present approach for determining the b/a value differs from that used in the previous ETEM study [23]. In that study, a full three-dimensional reverse Wulff construction was established for ZnO-supported Cu nanoparticles providing information about the Cu surface free energies as well as the Cu/ZnO interface energy for only three gas environments (H_2, H_2/H_2O, H_2/CO). This detailed method relies on ETEM images with atomic lattice resolution in two or more simultaneous crys-

Table 2
ETEM results for Cu nanoparticles supported on ZnO obtained during exposure to different gas environments (described in Table 1) at 2 mbar and 500 K. Experimental values for b/a are reported for different gas compositions characterized by Γ_{frozen} and $\Gamma_{\text{equilibrium}}$. The sign of b/a is positive or negative for particles with their Wulff point located above or below the Cu/ZnO interface, respectively. The b/a values are obtained as weighted averages with a standard deviation σ of N different particles in each sample. The Γ values given in parentheses are estimated values. The work of adhesion for the model catalyst W_{adh} is estimated by using the assumption that the Cu(111) facet interfaces with the ZnO substrate and that adsorbates on the Cu nanoparticles have a negligible effect on the surface free energies, as in [23]. That is, $\gamma_0 = \gamma_{(111)}$, where $\gamma_{(111)}$ is the free energy for the clean Cu(111) surface and is obtained from [31].

	Γ_{frozen}	$\Gamma_{\text{equilibrium}}$	N	b/a (σ)	W_{adh}/γ_0	W_{adh} (J/m^2)
50:50 CO:H_2	($>10^8$)	($>10^8$)	14	−0.01 (0.02)	1.01	2.0
5:95 CO:H_2	($>10^7$)	($>10^7$)	23	0.15 (0.01)	0.85	1.7
CO	Γ_2 ($>10^4$)	Γ_2 ($>10^4$)	38	0.11 (0.01)	0.89	1.7
H_2	Γ_1 ($>10^5$)	Γ_1 ($>10^5$)	19	0.14 (0.02)	0.86	1.7
Dry syngas	(10^5)	2×10^2	27	0.18 (0.02)	0.82	1.6
5:95 CO_2:H_2	(19)	27	27	0.15 (0.01)	0.85	1.7
50:50 CO_2:H_2	(1)	1	17	0.23 (0.03)	0.77	1.5
Wet syngas	1.8	3×10^{-2}	37	0.25 (0.02)	0.75	1.5
Wet 5:95 CO:H_2	($>10^4$)	2×10^{-2}	5	0.43 (0.05)	0.57	1.1
Wet H_2	$\Gamma_1 = 2$	$\Gamma_1 = 2$	12	0.25 (0.03)	0.75	1.5

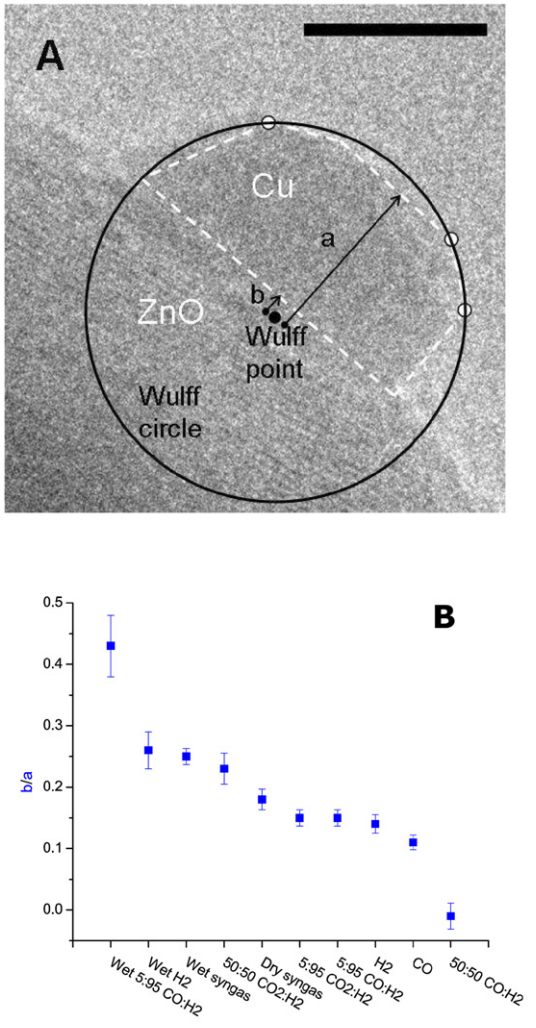

Fig. 6. ETEM image analysis and results. (A) The geometric Wulff circle analysis is illustrated for a profile-view ETEM image of a Cu nanoparticle on ZnO. Scale bar, 5 nm. Three white points at the edges of the particle define the Wulff circle (black circle) and its center (black dot). In the direction orthogonal to the particle–support interface, a defines the distance from the Wulff point to the top facet of the Cu nanoparticle and b defines the distance from the Wulff point to the Cu/ZnO interface. If the Wulff point is above the Cu/ZnO interface b is positive and if it is below the interface b is negative (as in this example). (B) Plot showing the weighted average b/a ratios versus gas composition (values given in Table 2) calculated via $\sum_i (x_i/\sigma_i^2)/\sum_i(\sigma_i^{-2})$. The error bars indicate the 1σ uncertainty calculated via $(\sum_i \sigma_i^{-2})^{-1/2}$.

tallographic directions implying that the Cu nanoparticle must be oriented with a zone-axis (almost) parallel to the electron beam in addition to having minimal overlap with the ZnO in the profile-view image. Finding such particles in the ETEM experiment is very time-consuming. As we here focus solely on the interface energy as a shape descriptor, fewer constraints on the particle orientation are needed facilitating the study of the gas-dependent nanoparticle shape in a broader range of gas environments. Still, a comparison of the work of adhesion obtained in the present work and in the previous study [23] shows an agreement for results obtained in comparable gas environments. Finally, it should be noted that the dynamic morphology of the Cu nanoparticles may be accompanied by effects of strain or Cu–Zn alloying depending on the reduction potential of the gas phase [28]. Such effects may also affect the methanol synthesis reaction but could not be identified in the present ETEM images.

4. Discussion

The present findings of a pretreatment-dependent transient methanol production are consistent with recent work by Wilmer and Hinrichsen [32]. They also observed that a pretreatment in H_2 did not result in a transient maximum in the methanol production and that a pretreatment in pure CO resulted in a much faster increase in the methanol production as compared to a pure H_2 pretreatment. However, following a CO pretreatment, a very small transient maximum in the methanol production was observed in [32] contrary to the present results (Fig. 3). The minor discrepancy in transient behavior is likely due to differences in the experimental setup, such as a higher signal-time broadening due to mass-transport through our reactor.

The present measurements of methanol production for the Cu/ZnO-based catalyst show that the pretreatment conditions couple to a transient methanol production and that a pretreatment gas containing both CO and H_2 results in a significant transient methanol production. This finding can qualitatively be explained by the gas-dependent Cu nanoparticle morphology observed in ETEM under the assumption that the Cu nanoparticle shape and methanol synthesis activity are related in accordance with [19]. In other words, the ETEM results show that more flat Cu nanoparticles are obtained in a H_2 and CO gas mixture giving an initially high methanol activity, and that more spherical particles are obtained during methanol synthesis gas conditions giving a subsequent activity decrease to a lower asymptotic level so a transient peak in the methanol production appears. The qualitative picture is consistent with previous explanations for the transient methanol production based on *in situ* EXAFS measurements [19]. Further-

more, the finding that the maximum transient methanol production followed a pretreatment in an intermediate mixture of H_2 and CO with a ratio close to unity is also consistent with the ETEM observations which show that the maximum flatness of the Cu nanoparticles is obtained under such gas conditions.

The finding that neither pure H_2 nor pure CO results in the most flat Cu nanoparticles is surprising because CO is more reducing gas than H_2. To address the question of why the Cu nanoparticles obtain the more flat shape in an intermediate H_2/CO mixture, we first examine the dynamic morphology model by Ovesen et al. [19]. The model describes the shape of the nanoparticles as the Wulff constructions based on the surface free energies of the clean Cu facets and an effective Cu/ZnO interface energy, γ^*. The model incorporates the effect of the gas phase composition on the Cu nanoparticle shape through the following reactions at the Cu/ZnO interface:

$$\begin{aligned} &H_2(g) + \text{Zn–O–Cu} \rightleftharpoons H_2O(g) + \text{Zn–}\square\text{–Cu},\\ &K_1 = \frac{p_{H_2O}}{p_{H_2}}\frac{[\text{Zn–}\square\text{–Cu}]}{[\text{Zn–O–Cu}]}; \end{aligned} \tag{6}$$

$$\begin{aligned} &CO(g) + \text{Zn–O–Cu} \rightleftharpoons CO_2(g) + \text{Zn–}\square\text{–Cu},\\ &K_2 = \frac{p_{CO_2}}{p_{CO}}\frac{[\text{Zn–}\square\text{–Cu}]}{[\text{Zn–O–Cu}]}; \end{aligned} \tag{7}$$

where K_1 and K_2 are equilibrium constants of the surface reduction reactions, and where [Zn–□–Cu]/[Zn–O–Cu] is the surface concentration of oxygen vacancies (reduced sites) in the Cu/ZnO interface divided by the concentration of unreduced sites. Using conservation of sites ([Zn–□–Cu] + [Zn–O–Cu] = 1) and assuming a linear relationship between γ^* and [Zn–□–Cu], Ovesen and coworkers showed that the effective interface energy, γ^*, and hence the nanoparticle shape depends on the gas phase composition according to:

$$\begin{aligned} \gamma^*/\gamma_0 &= \frac{1-\sqrt{(K_1\frac{P_{H_2}}{P_{H_2O}})(K_2\frac{P_{CO}}{P_{CO_2}})}}{1+\sqrt{(K_1\frac{P_{H_2}}{P_{H_2O}})(K_2\frac{P_{CO}}{P_{CO_2}})}}\\ &= \frac{1-\sqrt{K_1\Gamma_1K_2\Gamma_2}}{1+\sqrt{K_1\Gamma_1K_2\Gamma_2}}. \end{aligned} \tag{8}$$

The assumed linear relationship ([Zn–□–Cu] = $(1-\gamma^*/\gamma_0)/2$) means that a [Zn–□–Cu] = 0 results in no wetting of the surface by the nanoparticles (spherical shape), while a [Zn–□–Cu] = 1 gives complete wetting (mono-atomic high Cu discs). Based on this dynamic morphology model, the more flat Cu nanoparticles are obtained in gas environments with a high value of Γ. According to Eq. (8), Γ is maximized for $P_{H_2} \approx P_{CO}$ for a fixed total pressure and any finite denominator $P_{H_2O}P_{CO_2}$. Hence, the flattest particles are expected for a 50:50 CO:H_2 gas environment consistent with the ETEM observations. It is noted that in the ETEM setup, the denominator is determined by the finite base vacuum and gas cleanliness.

Fig. 4 illustrates the transient methanol production as a function of the H_2/CO ratio of the pretreatment gas composition. The abscissa is the gas mixture ratio and the points (right ordinate) show the corresponding, measured transient methanol production. Specifically, the highest transient activities are obtained for the Cu/ZnO catalyst that has been exposed to intermediate H_2/CO mixtures with 20–80% H_2. To examine the relation of the Cu nanoparticle shape obtained in such H_2/CO gasses and the transient methanol production, Fig. 4 also shows a fit of the shape descriptor γ^*/γ_0 (left ordinate) via Eq. (8) to the measured transient methanol production. Fig. 4 shows that the shape model and the measured transient methanol activity agree quite well and that the relation between the H_2/CO ratio of the pretreatment gas and the transient methanol production therefore qualitatively and quantitatively can be explained by the Cu/ZnO interface reactions in Eqs. (6) and (7).

To further characterize the Cu/ZnO interfacial reactions, the ETEM data are used to estimate the equilibrium constants K_1 and K_2. Thermodynamically, K_i is given by:

$$K_i = e^{-\Delta G_i/RT}, \quad i \in \{1,2\}, \tag{9}$$

where ΔG_i is the Gibbs free energy for the surface reduction reactions, Eqs. (6) and (7). Importantly, the ΔG values are associated with *surface* reactions and generally differ significantly from the corresponding *bulk* reactions. Neither CO nor H_2 can reduce bulk ZnO at 493 K and 1 bar because the Gibbs free energy for these reactions are $\Delta G_1 = 81$ kJ/mol and $\Delta G_2 = 61$ kJ/mol, respectively. For gas environments, where only one pair of CO/CO_2 or H_2/H_2O is present, a derivation similar to that of Eq. (8) gives:

$$\gamma^*/\gamma_0 = \frac{1-K_i\Gamma_i}{1+K_i\Gamma_i}, \tag{10}$$

where $i \in \{1,2\}$, K_i is defined by Eqs. (6) and (7) and Γ_i is defined by Eq. (5). Combining Eqs. (8) and (10) with the measured effective interface energy ($b/a \approx \gamma^*/\gamma_0$) in Table 2, the equilibrium constants, and the corresponding Gibbs free energies of the surface reactions, Eqs. (6) and (7), can be estimated. First, $K = K_1K_2$ is determined using the b/a data obtained for the Cu/ZnO catalyst in the 50:50 CO_2:H_2 mixture. For this gas mixture, Γ is unambiguous since $\Gamma_{\text{equilibrium}} = \Gamma_{\text{frozen}} = 1$. For $b/a = 0.23$ and $\Gamma = 1$ Eq. (8) gives $K = 0.39$ ($\Delta G = +3.8$ kJ/mol). To estimate K_1, the data from the wet H_2 environment are used in Eq. (10) resulting in: $K_1 = 0.3$ ($\Delta G_1 = +4.9$ kJ/mol). Finally, using $K = K_1K_2$ gives $K_2 = 1.3$ ($\Delta G_2 = -1.1$ kJ/mol). Thus it is possible to estimate the thermodynamics of the individual surface reduction reactions in Eqs. (6) and (7) based on the ETEM data. The ETEM-derived value for ΔG (3.8 kJ/mol) is also in good agreement with the estimate of Ovesen et al. which is in the interval $-2 \ldots +13$ kJ/mol [19]. Despite the differences between the applied methods and between the model catalyst (with 5% Cu) used in the present ETEM measurements and the industrial-type catalyst (with 50% Cu) used in the previous work [19], the agreement demonstrates that the model approach indeed captures the main trends of the Cu/ZnO interface reactions.

The dynamic morphology model describes the relation between the Cu nanoparticle shape and methanol activity in response to changes in gas composition. However, this model does not provide a direct physical reason for why mixtures of H_2 and CO are more reducing than the pure components and hence are leading to more flat Cu nanoparticles. It may be speculated that the origin of this synergy can be found in the mechanism for creation of oxygen vacancies in the ZnO surface. CO adsorbs weakly on Cu and on ZnO and might therefore by itself not be a good reducing agent. However, hydrogen dissociates on the Cu nanoparticles and might spill over to the ZnO surface. If hydrogen only partially reduces the ZnO surface—e.g., by forming ZnOH—but cannot remove the oxygen completely as H_2O, then hydrogen will not be able to reduce the ZnO surface by itself. However, hydrogen may via such a mechanism create a "point of attack" for CO thus removing the oxygen as CO_2. Further investigations, including modelling, are, however, necessary to elucidate this possible synergetic effect.

5. Conclusion

In summary:

- The transient over-production of methanol over a Cu/ZnO-based catalyst following pretreatments in H_2:CO mixtures has

for the first time been mapped out. A strong maximum in the methanol transient is found to follow pretreatments in ~1:1 H_2:CO mixtures.
- Surprisingly, a pretreatment with 1:1 H_2:CO gives more active Cu nanoparticles than a pretreatment with either pure H_2 or CO, suggesting a synergetic effect between the two gasses in the surface reduction of ZnO.
- An extensive ETEM study of Cu nanoparticles in a model catalyst in ten different gas mixtures representing both the pretreatment and methanol synthesis conditions has been carried out using a new method for analyzing particle shape.
- The ETEM results show that the pretreatment-dependent transient methanol production can be explained by a gas-dependent shape of Cu the nanoparticles in accordance with the model by Ovesen et al. [19].

The above observations should lead to a better understanding of the metal–support effects important for the Cu/ZnO system—particularly the shape-activity relationship. We have proposed a mechanism for the synergetic effect of the simultaneous presence of CO and H_2 in the pretreatment of the Cu/ZnO-based catalyst, but it remains to be confirmed by future *in situ* experiments.

Acknowledgments

The CTCI foundation, Taiwan, is gratefully acknowledged for participation in the establishment of the ETEM facility at Haldor Topsøe A/S. CINF is funded by the Danish National Research Foundation.

References

[1] G.A. Olah, Angew. Chem. Int. Ed. 44 (18) (2005) 2636–2639.
[2] M. Bowker, H. Houghton, K.C. Waugh, J. Chem. Soc. Faraday Trans. 1 77 (1981) 3023–3036.
[3] G.C. Chinchen, P.J. Denny, D.G. Parker, M.S. Spencer, D.A. Whan, Appl. Catal. 30 (2) (1987) 333–338.
[4] J. Nerlov, S. Sckerl, J. Wambach, I. Chorkendorff, Appl. Catal. A 191 (1–2) (2000) 97–109.
[5] P.B. Rasmussen, M. Kazuta, I. Chorkendorff, Surf. Sci. 318 (3) (1994) 267–280.
[6] P.B. Rasmussen, P.M. Holmblad, T. Askgaard, C.V. Ovesen, P. Stoltze, J.K. Nørskov, I. Chorkendorff, Catal. Lett. 26 (3–4) (1994) 373–381.
[7] J. Yoshihara, C.T. Campbell, J. Catal. 161 (2) (1996) 776–782.
[8] J. Nakamura, I. Nakamura, T. Uchijima, T. Watanabe, T. Fujitani, Stud. Surf. Sci. Catal. 101B (1996) 1389–1399.
[9] J.B. Hansen, Handbook of Heterogeneous Catalysis, vol. 4, Wiley–VCH, New York, 1997, pp. 1856–1876.
[10] N.-Y. Topsøe, H. Topsøe, Top. Catal. 8 (1999) 267–270.
[11] M.M. Günther, T. Ressler, B. Bems, C. Büscher, T. Genger, O. Hinrichsen, M. Muhler, R. Schlögl, Catal. Lett. 71 (1–2) (2001) 37–44.
[12] I. Kasatkin, P. Knurr, A. Kniep, B. Trunschke, T. Ressler, Angew. Chem. 119 (38) (2007) 7465–7468.
[13] M.M. Viitanen, W.P.A. Jansen, R.G.v. Welzenis, H.H. Brongersma, D.S. Brands, E.K. Poels, A. Bliek, J. Phys. Chem. B Condens. Phase 103 (29) (1999) 6025–6029.
[14] J. Fujitani, J. Nakamura, Catal. Lett. 56 (2–3) (1998) 119–124.
[15] R.N. d'Alnoncourt, M. Kurtz, H. Wlimer, E. Lffler, V. Hagen, J. Shen, M. Muhler, J. Catal. 220 (1) (2003) 249–253.
[16] B.S. Clausen, J. Schiøtz, L. Gråbæk, C.V. Ovesen, K.W. Jacobsen, J.K. Nørskov, H. Topsøe, Top. Catal. 1 (3–4) (1994) 367–376.
[17] J.D. Grunwaldt, A.M. Molenbroek, N.Y. Topsøe, H. Topsøe, B.S. Clausen, J. Catal. 194 (2000) 452–460.
[18] B.S. Clausen, H. Topsøe, Catal. Today 9 (1–2) (1991) 189–196.
[19] C.V. Ovesen, B.S. Clausen, J. Schiøtz, P. Stoltze, H. Topsøe, J.K. Nørskov, J. Catal. 168 (1997) 133–142.
[20] M. Muhler, E. Törnqvist, L.P. Nielsen, B.S. Clausen, H. Topsøe, Catal. Lett. 25 (1–2) (1994) 1–10.
[21] E.G. Derouane, R.T.K. Baker, J.A. Dumesic, R.D. Sherwood, J. Catal. 69 (1) (1981) 101–110.
[22] S. Giorgio, S.S. Joao, S. Nitsche, D. Chaudanson, G. Sitja, C.R. Henry, Ultramicroscopy 106 (6) (2006) 503–507.
[23] P.L. Hansen, J.B. Wagner, S. Helveg, J.R. Rostrup-Nielsen, B.S. Clausen, H. Topsøe, Science 195 (2002) 2053–2055.
[24] B. Kasemo, Rev. Sci. Instrum. 50 (12) (1979) 1602–1604.
[25] B.S. Rasmussen, P.E.H. Nielsen, J. Villadsen, J.B. Hansen, Preparation of Catalysts, vol. IV, Elsevier, Amsterdam, 1987, p. 875.
[26] P.L. Hansen, S. Helveg, A.K. Datye, Adv. Catal. 50 (2006) 77–95.
[27] I. Kasatkin, B. Kniep, T. Ressler, Phys. Chem. Chem. Phys. 9 (2007) 878–883.
[28] J.B. Wagner, P.L. Hansen, A.M. Molenbroek, H. Topsøe, B.S. Clausen, S. Helveg, J. Phys. Chem. B 107 (2003) 7753–7758.
[29] G. Wulff, Z. Kristallogr. 34 (1901) 449–530.
[30] W.L. Winterbottom, Acta Metall. 15 (303) (1967) 303–310.
[31] L. Vitos, A.V. Ruban, H.L. Skriver, J. Kollar, Surf. Sci. 411 (1998) 186–202.
[32] H. Wilmer, O. Hinrichsen, Catal. Lett. 82 (1–2) (2002) 117–122.